NANO LETTERS

Letter

pubs.acs.org/NanoLett

Stable Alkali Metal Ion Intercalation Compounds as Optimized Metal Oxide Nanowire Cathodes for Lithium Batteries

Yunlong Zhao,[†,∥,#] Chunhua Han,[†,#] Junwei Yang,[‡,#] Jie Su,[§] Xiaoming Xu,[†] Shuo Li,[†] Lin Xu,[∥] Ruopian Fang,[†] Hong Jiang,[⊥] Xiaodong Zou,*[,§] Bo Song,*[,‡] Liqiang Mai,*[,†] and Qingjie Zhang[†]

[†]State Key Laboratory of Advanced Technology for Materials Synthesis and Processing, Wuhan University of Technology, Wuhan 430070, China

[‡]Shanghai Institute of Applied Physics, Chinese Academy of Sciences, Shanghai 201800, China

[§]Inorganic and Structural Chemistry and Berzelii Center EXSELENT on Porous Materials, Department of Materials and Environmental Chemistry, Stockholm University, Stockholm SE−106 91, Sweden

[∥]Department of Chemistry and Chemical Biology, Harvard University, Cambridge, Massachusetts 02138, United States

[⊥]Beijing National Laboratory for Molecular Sciences, State Key Laboratory of Rare Earth Materials Chemistry and Applications, Institute of Theoretical and Computational Chemistry, College of Chemistry and Molecular Engineering, Peking University, Beijing 100871, China

Supporting Information

ABSTRACT: Intercalation of ions in electrode materials has been explored to improve the rate capability in lithium batteries and supercapacitors, due to the enhanced diffusion of Li^+ or electrolyte cations. Here, we describe a synergistic effect between crystal structure and intercalated ion by experimental characterization and ab initio calculations, based on more than 20 nanomaterials: five typical cathode materials together with their alkali metal ion intercalation compounds A−M−O (A = Li, Na, K, Rb; M = V, Mo, Co, Mn, Fe−P). Our focus on nanowires is motivated by general enhancements afforded by nanoscale structures that better sustain lattice distortions associated with charge/discharge cycles. We show that preintercalation of alkali metal ions in V−O and Mo−O yields substantial improvement in the Li ion charge/discharge cycling and rate, compared to A−Co−O, A−Mn−O, and A−Fe−P−O. Diffraction and modeling studies reveal that preintercalation with K and Rb ions yields a more stable interlayer expansion, which prevents destructive collapse of layers and allow Li ions to diffuse more freely. This study demonstrates that appropriate alkali metal ion intercalation in admissible structure can overcome the limitation of cyclability as well as rate capability of cathode materials, besides, the preintercalation strategy provides an effective method to enlarge diffusion channel at the technical level, and more generally, it suggests that the optimized design of stable intercalation compounds could lead to substantial improvements for applications in energy storage.

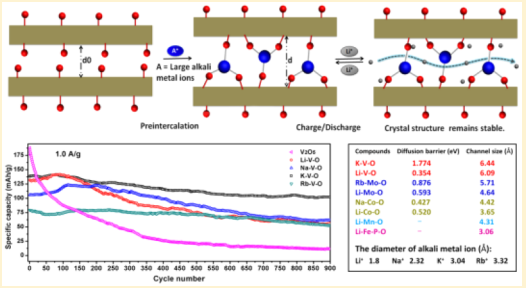

KEYWORDS: *Alkali metal ion intercalation, metal oxide nanowire cathodes, rotation electron diffraction, ab initio calculations, synergistic stabilizing effect*

Large-scale rechargeable lithium batteries have the potential to meet the demands of electric vehicles, including hybrids, plug-in hybrids, and full-electric vehicles.[1−4] Despite continued improvements in the performance of rechargeable lithium batteries, their application and/or impact remain limited by energy density, cycling stability, and rate performance.[5−7] For example, conventional layered metal oxide (MO) cathode materials, such as $LiCoO_2$, $LiNiO_2$, and $LiMnO_2$, do not meet ideal needs due to their relatively low specific capacities.[8,9] Thus, it is necessary to further improve or develop novel cathode materials to optimize the overall electrochemical behavior of battery systems.

As a prototypical layered MO, vanadium oxides have been studied for ca. 40 years as potential cathode materials for battery systems.[10,11] The facile distortion of V−O octahedra leads to the formation of a large variety of vanadium oxide structures, which, together with the rich chemical valences of vanadium, can result in an intercalated lithium level with capacity exceeding 300 mAh/g.[12−15] However, structural changes associated with lithium intercalation/deintercalation (discharge/charge) can disorder and ultimately transform the material to an inactive state, which leads to a poor cycling stability[16] (Figure S1, Supporting Information).

One general approach to overcome this problem is to use nanoscale structures, for example, nanowires, that can reduce the lithium ion diffusion length and better sustain lattice strains, although nanostructures with a large electrolyte/electrode

Received: January 23, 2015
Published: February 5, 2015

DOI: 10.1021/acs.nanolett.5b00284
Nano Lett. 2015, 15, 2180−2185

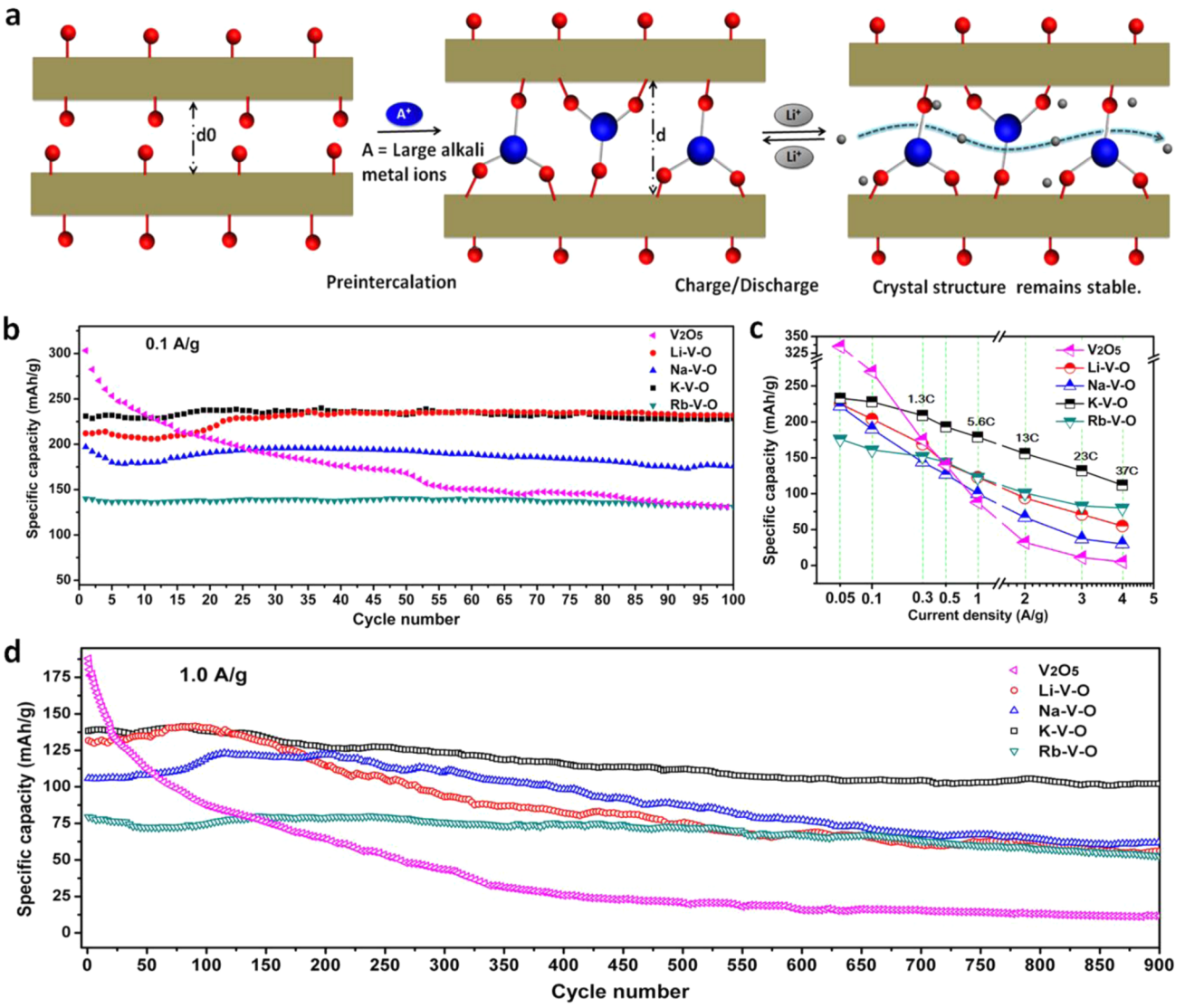

Figure 1. Schematic representation and electrochemical properties of large alkali metal ion intercalation. (a) Schematic representation of large alkali metal ion intercalation. (b) Cycling performance of A−V−O nanowires formed by preintercalating large alkali metal ions into vanadium oxides with a charge/discharge rate of 0.1 A/g. (c) Rate performance of A−V−O nanowires. A−V−O nanowires are cycled at various rates from 0.05 to 4.0 A/g. Here *nC* denotes the rate at which a full charge or discharge takes $1/n$ hours. (d) Cycling performance of A−V−O nanowires at the charge/discharge rate of 1.0 A/g.

surface area may require greater attention to interfacial stability.[6,17,18] Another approach is to use preintercalation to enhance the structural stability during the charge/discharge processes. In previously studies, we find that preintercalation of electrolyte cations could enhance the cycling stability and rate capability of layered MO cathode during the charge−discharge processes.[19−22] Lukatskaya et al. intercalated ions in layered titanium carbide, enlarged the diffusion channels and revealed the improved rate capability.[23] However, the mechanisms for the roles of preintercalation and the changes of modified interlayer diffusion are still poorly understood, which limits further controllable optimization and development of layered electrode materials.

To overcome the limitation mentioned above layered MO cathode structures, we systemically investigated vanadium-based nanowires intercalated with alkali metal ions (A = Li, Na, K, Rb). We hypothesize that preintercalation of appropriate alkali metal ions (blue spheres, Figure 1a) larger than Li^+ may stabilize the MO interlayer structure and enlarge the diffusion channel (Figure 1a), which prevent destructive structural changes and facilitate Li ion diffusion during charge−discharge processes, leading to enhancement of cycling stability as well as rate capability. The proposed scheme to stabilize interlayer structure by large alkali metal ion intercalation in our model is distinct from previous intercalation studies.[21,23−28]

To explore the influence of preintercalation on electrochemical performance, we prepared A−V−O nanowires preintercalated with A (= Li, Na, K, Rb) alkali metal ions, and tested their cycling and rate behaviors. The capacity retention after 100 cycles at 0.1 A/g (Figure 1b) significantly increases from 37.6% for baseline V_2O_5 to over 95% for preintercalated A−V−O, although the preintercalated compounds have lower initial capacities than V_2O_5. A comparison of rate performance (Figure 1c) shows that even at the highest rate (~37C), the capacity of K−V−O, ~110 mAh/g, is much higher than that of V_2O_5 or other A−V−O. Additional studies at a rate of 1.0 A/g and for prolonged deep charge−discharge up to 900 cycles (Figure 1d) highlight the substantial

DOI: 10.1021/acs.nanolett.5b00284
Nano Lett. 2015, 15, 2180−2185

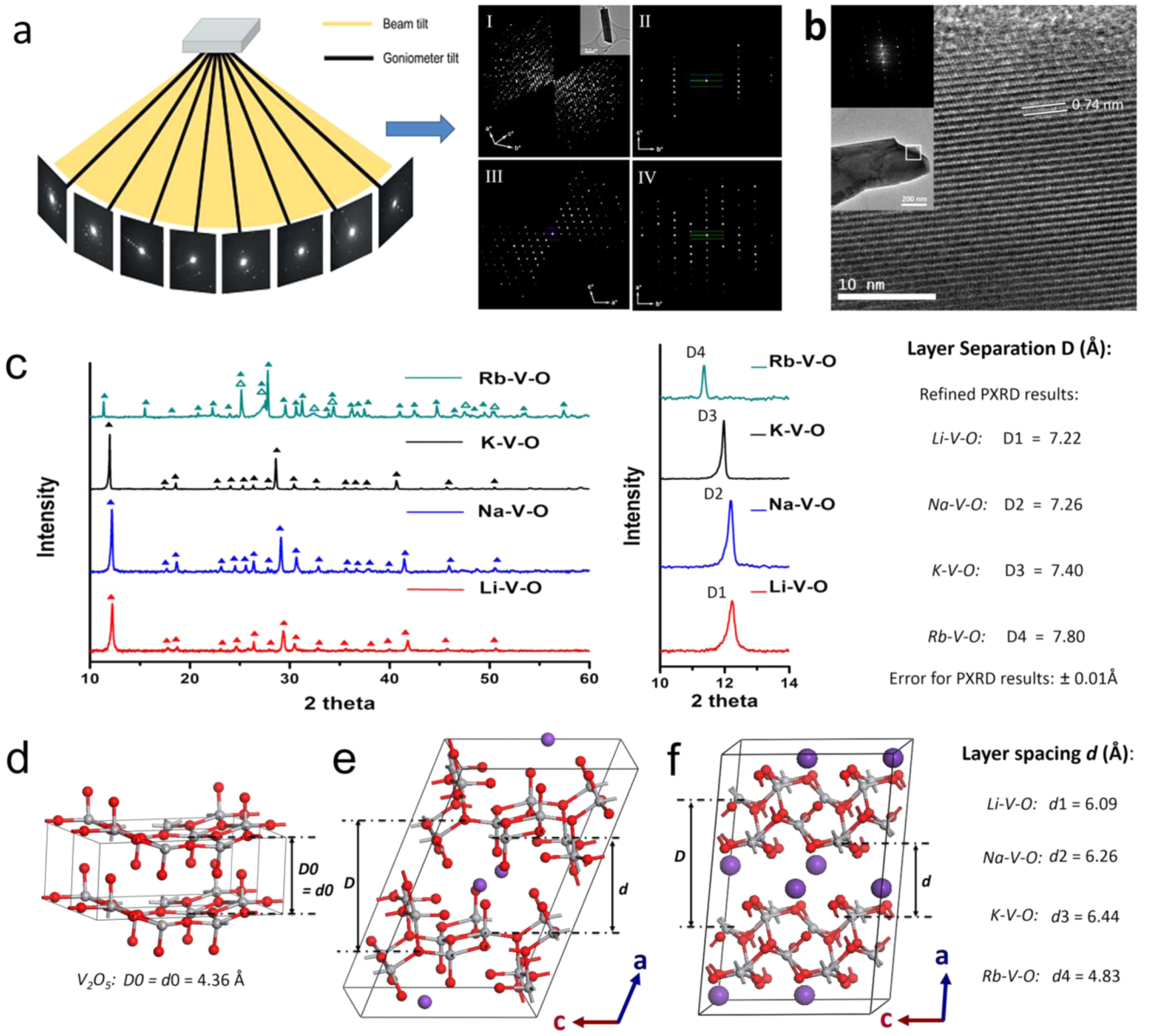

Figure 2. RED, PXRD, and DFT analysis of A–V–O nanowires. (a) (Left) Schematic representation of the concept of the rotation electron diffraction (RED) method. (Right) The rotation electron diffraction (RED) data of K–V–O nanowires. I represents reconstructed 3D reciprocal lattice of K–V–O nanowires from RED data, and II–IV represent 2D slices cut from the reconstructed 3D reciprocal lattice showing the 0*kl*, *h*0*l*, and *hk*0 plane, respectively. (b) HRTEM image of K–V–O nanowire showing the lattice fringes about 7.4 Å, corresponding to d_{200} for K–V–O. The insets are TEM image and FFT pattern on selected area. (c) (Left) PXRD patterns of A–V–O nanowires. (Right) Refined PXRD of the interplanar layer separations. (d–f) Illustration of the crystal structure of V_2O_5, A–V_6O_{15} (A = Li, Na, K) and RbV_3O_8, respectively. Li–V_6O_{15}, Na–V_6O_{15} and K–V_6O_{15} are isostructural. The red, gray, and purple balls represent the O, V, A, or Rb atoms, respectively. Layer separation *D* represents the repeat distance in crystal structure, while layer spacing *d* denotes the distance between top and bottom of the space for Li ions intercalating in initial diffusion channel.

improvement afforded by the preintercalated A–V–O compounds compared to baseline V_2O_5 (capacity retention: K–V–O ≥ Rb–V–O > Na–V–O > Li–V–O ≫ V_2O_5). Remarkably, the K–V–O electrodes exhibit maximal capacity retention: After 900 cycles the K–V–O electrode retains 76% of 139 mAh/g compared to 39% for Li–V–O and 50% for Na–V–O under the same conditions. In addition, we tested the cyclic voltammetric (CV) performance of V_2O_5 and A–V–O (Figure S2, Supporting Information). Comparison of the CV curve areas between V_2O_5 and A–V–O shows a decrease after alkali metal ion intercalation due to the partial occupation of total available intercalation sites for Li ions during discharging. Notably, the amplitude of the cathodic peak at ∼1.85 V, corresponding only to the irreversible phase transition,[14] is reduced for the preintercalated materials (amplitude of the irreversible cathodic peak: K–V–O ≤ Rb–V–O < Na–V–O < Li–V–O ≪ V_2O_5). This distinguishing property for K–V–O further supports that preintercalation of large alkali ions can greatly improve intrinsic diffusion and reversibility of Li ion intercalation/deintercalation during the discharge/charge cycles.

To identify the phase(s) present in the materials and determine the unit cell parameters, we applied our newly developed rotation electron diffraction (RED) method.[29] The

DOI: 10.1021/acs.nanolett.5b00284
Nano Lett. 2015, 15, 2180–2185

advantage of the RED method compared to powder X-ray diffraction or conventional electron diffraction is that an almost complete 3D electron diffraction dataset can be collected from a nanosized crystal in a short time (<1 h) (Figure 2a); then the reconstructed 3D reciprocal lattice and 2D slices 0*kl*, *h*0*l*, and *hk*0 (Figures 2a and S4b−7b, Supporting Information) could be reconstructed directly from the RED data, from which the unit cell parameters and possible space groups were determined. HRTEM images revealed that the layers are in parallel to the nanowires (Figures 2b and S4d−6d, Supporting Information). Detailed TEM analyses of A−V−O are given in Supporting Information Part 3. The PXRD patterns (Figures 2c, S4a−S6a, and S7c, Supporting Information) show that the materials correspond to $Li_{0.7}V_6O_{15}$ for Li−V−O, $Na_{0.9}V_6O_{15}$ for Na−V−O, and $K_{0.7}V_6O_{15}$ for K−V−O. In Rb−V−O, RbV_3O_8 is the major phase, and an unknown minor Rb−V−O phase was found by RED (Figure S7, Supporting Information). The unit cell parameters determined by RED and refined by Pawley fitting show that the A−V−O (A = Li, Na, K) phases are monoclinic and isostructural (Figure 2e and Tables S1 and S3, Supporting Information) and are different from the original V_2O_5 structure (Figures 2d and S8, Supporting Information), while RbV_3O_8 exhibits another layered structure (Figures 2f and S7 and Table S7, Supporting Information). The PXRD results match very well with the RED results. The layer separation *D*, defined as d_{200} for Li-/Na-/K−V−O and d_{100} for Rb−V−O (Figure 2c, right), increases with increasing size of the cations (Li, 7.22 Å; Na, 7.26 Å; K, 7.40 Å; Rb, 7.80 Å) and is significantly higher than that of V_2O_5 (4.36 Å), suggesting a significant lattice expansion after large alkali metal ion intercalation.

To further understand these structural changes and their effects on the rate behaviors, we estimate the diffusion channel sizes in the A−V−O materials from the models obtained by RED and PXRD using an ab initio method based on the density functional theory (DFT). We define layer spacing *d* as the distance between top and bottom of the space for Li^+ transport by excluding the thickness of the intralayer (Figure 2d−f). K−V−O exhibits the widest layer spacing. Since Ceder group demonstrates that the lattice and size of Li ion diffusion channel is critical to rate capability,[30−32] the most expansive diffusion channel resulted by preintercalation with K^+ can lead to the greatest enhancement of rate capability, consistent with the electrochemical performance.

To reveal the poorly understood mechanism underlying the substantial improvement in cycling stability after large metal ion preintercalation, we studied the cyclability of A−V−O structure based on the diffusion behavior (via diffusion barrier, $E_{barrier}$) of preintercalated A ions in A−V−O for a charge state without considering lithiated structure. By DFT method, the $E_{barrier}$ of the preintercalated A ion between two neighboring sites was calculated using $A_7V_{48}O_{120}$ (two unit cells) for A−V−O with A = Li, Na, K, and $Rb_{15}V_{48}O_{120}$ (four unit cells) for Rb−V−O (see the details in Section 6 in Part 3 of the Supporting Information). For A = Li, Na to K, $E_{barrier}$ increases with A ion size increasing (Figure 3a). To reveal the nature under this order, their molecular configurations are traced back. It is found that the special interaction between preintercalated A ions and single-connected terminal oxygen atoms on the surface of interlayer (Figure 2e, and for zoom-in image, Figure S10, Supporting Information) plays a key role in $E_{barrier}$: on the premise of thermodynamics stability, because of noncovalent interaction between the preintercalated A ions and the terminal

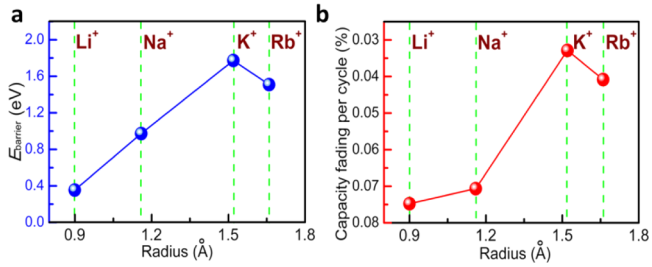

Figure 3. DFT analysis and electrochemical properties in crystal structure of A−V−O nanowires. (a) Diffusion barrier ($E_{barrier}$) of A in A−V−O obtained from ab initio calculations. (b) Capacity fading per cycle vs the radius of different preintercalated ions at a rate of 1.0 A/g.

oxygen atoms of distortable V−O single bond, the larger the A ion is to diffuse in between the layers, the greater the distortion of the V−O single bond, which leads to a large diffusion barrier for large metal ions. Therefore, the diffusion of large K ion in between the two layers is suppressed, which in return acts on the layered structure, hinders the relative slippage between the two parallel layers, and prevents the destructive distortion of the structure. Meanwhile, the anchored K ions between interlayers also support two layers and protect the layered structure from collapse vertically. Namely, K ions can act as "pillars" between two layers[33] (Figure 1a), which results in a more stable interlayer structure in K−V−O than in Li−V−O and Na−V−O during charge−discharge processes, and then leads to the highest cyclability of K−V−O. The $E_{barrier}$ of Rb in Rb−V_3O_8 is lower than that of K in K−V−O, which is attributed to the structural difference (Figures 2f and S7, Supporting Information). However, because of ionic size, the barrier of Rb in Rb−V_3O_8 is still higher than those of Na in Na−V−O and Li in Li−V−O. These theoretical observations indicate an order of stability in charge−discharge processes: K−V−O > Rb−V−O > Na−V−O > Li−V−O, which is well consistent with the order of the cyclability experimentally (Figure 3b). Remarkably, all of the above results suggest that alkali metal ions are selectively captured in A−V−O by the V−O layers according to the ionic size: The large metal ions are anchored by the layers, while the small metal ions (Li^+) are allowed to diffuse freely in between the layers.

To validate the above theoretical results, we used atomic absorption spectroscopy to analyze the deintercalation of A ions from the electrode material during cycling. Measurements made on a mixture of Na−V−O and K−V−O nanowires with an initial atomic ratio of 3.3% Na and 96.7% K show that after 900 cycles at 1.0 A/g the percentages of ions in the electrolyte are 60.7% Na and 39.3% K. Assuming all of the Na ions in the original nanowire mixture deintercalate into the electrolyte, we can place an upper bound on the 1.7% K ions deintercalated using the final solution ratio. Notably, this analysis shows that less than 2% K is lost, thus confirming that the K ions (vs Na ions) can be selectively anchored in between V−O layers, then yielding more stabilized interlayers (further supported in XRD characterization during cycling, Figure S11, Supporting Information).

Finally, to further present the synergistic stabilizing effect observed in A−V−O (namely, the V−O layers can selectively capture A ions according to the ionic size, and the large alkali metal ions can act as pillars in between layers to yield a stable interlayer expansion and prevent the destructive distortion or collapse of the V−O layers in charge−discharge processes), we

DOI: 10.1021/acs.nanolett.5b00284
Nano Lett. 2015, 15, 2180−2185

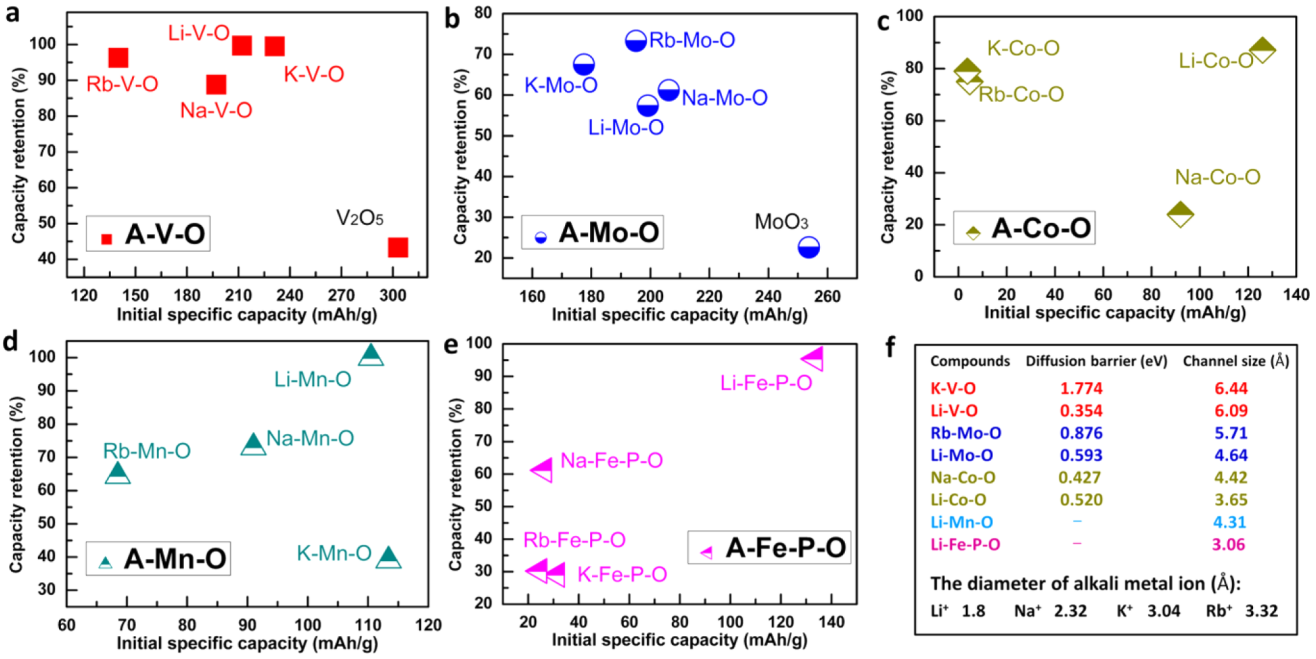

Figure 4. Comparison of initial specific capacity and capacity retention of compounds as cathodes before and after alkali metal ion intercalation; all data are based on our experiments (details are shown in Supporting Information). (a–e) A–M–O (A = Li, Na, K, Rb; M = V, Mo, Co, Mn, Fe–P) are tested at charge/discharge rate of 0.1 A/g for 100 cycles. (f) The diffusion barrier of alkali metal A ions and the size of ion diffusion channel of typical A–M–O cathode materials and the diameter of alkali metal ion.

explored the influence of preintercalation on the cycling stability of other typical cathode materials: layered MoO_3 and $LiCoO_2$, the spinel-type $LiMn_2O_4$ and olivine-type $LiFePO_4$. Their alkali metal ion intercalation compounds are labeled as A–M–O (A= Li, Na, K, Rb; M = Mo, Co, Mn, Fe–P). Considering the limitations from electronic conductance and ionic diffusion of the different cathodes, low current density of 0.1 A/g was applied for comparison.

For layered A–Mo–O (Figures 4b and S12, Supporting Information) after preintercalating large alkali metal ions, i.e., K and Rb ions, the cycling stability increased significantly, similar to that of A–V–O. As suggested by crystallographic and theoretical analysis, this clearly enhanced performance is attributed to the appropriate interactions between A ions and single-connected terminal oxygen atoms on the surface of layers similar to the interaction of A ions with the terminal oxygen atoms in A–V–O (see Figures S12c and S10, Supporting Information), which can provide a high diffusion barrier for large alkali metal ions (Figure 4f, 0.876 eV of Rb^+) and a low barrier for small alkali metal ions Li (Figure 4f, 0.593 eV). Therefore, preintercalation with A ions also presents selective capture, while large A ions play a pillar effect in between the layers.

For A–Co–O (Figures 4c and S13, Supporting Information), although preintercalation of Na ions can significantly enlarge the layer separation (Figure S13a, Supporting Information; Li–Co–O, 4.55 Å; Na–Co–O, 5.08 Å), the cycling stability is reduced, contrary to the behavior of A–V–O materials where the retention clearly increases. This can be attributed to that the $E_{barrier}$ of Na ion in Na–Co–O (0.427 eV) is lower than Li in Li–Co–O (0.520 eV). As shown in Figure S13b, Supporting Information, the oxygen atoms on the surface layer are triconnected and less flexible compared to the single-connected terminal oxygen atoms on the layer surface of A–V–O (see Figure S14, Supporting Information). Therefore, the Co–O layered structure cannot provide a large diffusion barrier for large A ions in between the layers like the A–V–O structure, resulting in a different diffusion behavior of A ions in A–Co–O from A–V–O. Incorporation of the larger K or Rb ions led to an inactive electrode material, and the structures are no longer layered. Thus, the proposed synergistic stabilizing effect depends on the layer surface configuration. Furthermore, if an appropriate way is found to modify the surface of layers, it can be expected to introduce the effect to the layered structure (such as A–Co–O) and then greatly improve the cycling stability (like A–V–O and A–Mo–O).

For spinel-type A–Mn–O (Figures 4d and S15, Supporting Information) and olivine-type A–Fe–P–O (Figures 4e and S16, Supporting Information), intercalation of large alkali metal ions (e.g., K^+ or Rb^+) leads to the serious decrease in capacity or/and cyclability (Figure 4d,e), although the performance of Na–Mn–O is acceptable. Actually, intercalation of large alkali metal ions in A–Mn–O and A–Fe–P–O will block the narrow diffusion channel (see Figure 4f) and/or destroy the intrinsic structures, which can be attributed to the stable small channel size of ion diffusion vs large alkali metal ion intercalation.

Combining the above characterization and analysis, we conclude that the appropriate large alkali metal ion intercalation in admissible crystal structure (without structure damage) can enlarge and stabilize diffusion channel, leading to the enhancement of cycling stability as well as rate performance.

In summary, we have systematically investigated alkali metal ion intercalation compounds as optimized cathodes for lithium batteries based on electrochemical tests, diffraction characterization, and ab initio calculations. It is found that appropriate alkali metal ion intercalation in admissible layered structure can overcome the limitation of cyclability as well as rate capability. This is attributed to the synergistic stabilizing effect between the intercalated ions and the layers with appropriate layer–surface configuration in charge–discharge processes together

DOI: 10.1021/acs.nanolett.5b00284
Nano Lett. 2015, 15, 2180–2185

with the enlarged layer spacing. Besides, such strategy provides a facile and effective method to regulate the diffusion channel of some intercalation compounds at the technical level, which are promising and important for the future design and optimization of intercalation compounds as cathodes for rechargeable lithium- and other metal-based or metal ion batteries. More generally, this effect of preintercalation could be widely applied in energy storage and even in the fields of novel stable material design, artificial transmembrane ion channels, environmental treatment, and other applications.

■ ASSOCIATED CONTENT

Supporting Information

Additional information and figures. This material is available free of charge via the Internet at http://pubs.acs.org.

■ AUTHOR INFORMATION

Corresponding Authors

*E-mail: mlq518@whut.edu.cn.
*E-mail: bosong@sinap.ac.cn.
*E-mail: xzou@mmk.su.se.

Author Contributions

#These authors contributed equally to this work.

Notes

The authors declare no competing financial interest.

■ ACKNOWLEDGMENTS

This work was supported by National Basic Research Program of China (2013CB934103, 2012CB933003, and 2010CB934504), National Natural Science Foundation of China (51302203, 51272197, and 11174310), the International Science and Technology Cooperation Program of China (2013DFA50840), the National Natural Science Fund for Distinguished Young Scholars (51425204), the Fundamental Research Funds for the Central Universities (WUT:143201003), the Knowledge Innovation Program of the Chinese Academy of Sciences, and the Shanghai Supercomputer Center of China. The structure characterization by PXRD and TEM was supported by the Swedish Research Council (VR), the Swedish Governmental Agency for Innovation Systems (VINNOVA), and the Knut and Alice Wallenberg Foundation through a grant for purchasing the TEM and the project grant 3DEM-NATUR. Special thanks to Professor C. M. Lieber of Harvard University for his careful supervision, strong support, and stimulating discussion.

■ REFERENCES

(1) Dunn, D.; Kamath, H.; Tarascon, J.-M. *Science* **2011**, *334*, 928−935.
(2) Chu, S.; Majumdar, A. *Nature* **2012**, *488*, 294−303.
(3) Armand, M.; Tarascon, J.-M. *Nature* **2008**, *451*, 652−657.
(4) Aricò, A. S.; Bruce, P.; Scrosati, B.; Tarascon, J.-M.; Van Schalkwijk, W. *Nat. Mater.* **2005**, *4*, 366−377.
(5) Goodenough, J. B.; Kim, Y. *Chem. Mater.* **2009**, *22*, 587−603.
(6) Bruce, P. G.; Scrosati, B.; Tarascon, J. M. *Angew. Chem., Int. Ed.* **2008**, *47*, 2930−2946.
(7) Sun, Y.-K.; Chen, Z.; Noh, H.-J.; Lee, D.-J.; Jung, H.-G.; Ren, Y.; Wang, S.; Yoon, C. S.; Myung, S.-T.; Amine, K. *Nat. Mater.* **2012**, *11*, 942−947.
(8) Whittingham, M. S. *Chem. Rev.* **2004**, *104*, 4271−4302.
(9) Tarascon, J.-M.; Armand, M. *Nature* **2001**, *414*, 359−367.
(10) Chernova, N. A.; Roppolo, M.; Dillon, A. C.; Whittingham, M. S. *J. Mater. Chem.* **2009**, *19*, 2526−2552.
(11) Cheng, F.; Chen, J. *J. Mater. Chem.* **2011**, *21*, 9841−9848.
(12) Mai, L.; Xu, L.; Han, C.; Xu, X.; Luo, Y.; Zhao, S.; Zhao, Y. *Nano Lett.* **2010**, *10*, 4750−4755.
(13) Wu, C.; Feng, F.; Xie, Y. *Chem. Soc. Rev.* **2013**, *42*, 5157−5183.
(14) Liu, Y.; Clark, M.; Zhang, Q.; Yu, D.; Liu, D.; Liu, J.; Cao, G. *Adv. Energy Mater.* **2011**, *1*, 194−202.
(15) Yang, S.; Gong, Y.; Liu, Z.; Zhan, L.; Hashim, D. P.; Ma, L.; Vajtai, R.; Ajayan, P. M. *Nano Lett.* **2013**, *13*, 1596−1601.
(16) Chan, C. K.; Peng, H.; Twesten, R. D.; Jarausch, K.; Zhang, X. F.; Cui, Y. *Nano Lett.* **2007**, *7*, 490−495.
(17) Zhou, W.; Dai, X.; Fu, T. M.; Xie, C.; Liu, J.; Lieber, C. M. *Nano Lett.* **2014**, *14*, 1614−1619.
(18) Wu, Y.; Xiang, J.; Yang, C.; Lu, W.; Lieber, C. M. *Nature* **2004**, *430*, 61−65.
(19) Mai, L. Q.; Hu, B.; Chen, W.; Qi, Y.; Lao, C.; Yang, R.; Dai, Y.; Wang, Z. L. *Adv. Mater.* **2007**, *19*, 3712−3716.
(20) Tian, X.; Xu, X.; He, L.; Wei, Q.; Yan, M.; Xu, L.; Zhao, Y.; Yang, C.; Mai, L. *J. Power Sources* **2014**, *255*, 235−241.
(21) Mai, L.; Li, H.; Zhao, Y.; Xu, L.; Xu, X.; Luo, Y.; Zhang, Z.; Ke, W.; Niu, C.; Zhang, Q. *Sci. Rep.* **2013**, *3*, 1718−1726.
(22) Mai, L.; Tian, X.; Xu, X.; Chang, L.; Xu, L. *Chem. Rev.* **2014**, *114*, 11828−11862.
(23) Lukatskaya, M. R.; Mashtalir, O.; Ren, C. E.; Dall'Agnese, Y.; Rozier, P.; Taberna, P. L.; Naguib, M.; Simon, P.; Barsoum, M. W.; Gogotsi, Y. *Science* **2013**, *341*, 1502−1505.
(24) Mashtalir, O.; Naguib, M.; Mochalin, V. N.; Dall'Agnese, Y.; Heon, M.; Barsoum, M. W.; Gogotsi, Y. *Nat. Commun.* **2013**, *4*, 1716.
(25) Xie, Y.; Naguib, M.; Mochalin, V. N.; Barsoum, M. W.; Gogotsi, Y.; Yu, X.; Nam, K.-W.; Yang, X.-Q.; Kolesnikov, A. I.; Kent, P. R. *J. Am. Chem. Soc.* **2014**, *136*, 6385−6394.
(26) Yang, X.; Cheng, C.; Wang, Y.; Qiu, L.; Li, D. *Science* **2013**, *341*, 534−537.
(27) Augustyn, V.; Come, J.; Lowe, M. A.; Kim, J. W.; Taberna, P.-L.; Tolbert, S. H.; Abruña, H. D.; Simon, P.; Dunn, B. *Nat. Mater.* **2013**, *12*, 518−522.
(28) Mefford, J. T.; Hardin, W. G.; Dai, S.; Johnston, K. P.; Stevenson, K. J. *Nat. Mater.* **2014**, *13*, 726−732.
(29) Wan, W.; Sun, J.; Su, J.; Hovmoller, S.; Zou, X. *J. Appl. Crystallogr.* **2013**, *46*, 1863−1873.
(30) Kang, K.; Meng, Y. S.; Breger, J.; Grey, C. P.; Ceder, G. *Science* **2006**, *311*, 977−980.
(31) Kang, K.; Ceder, G. *Phys. Rev. B* **2006**, *74*, 094105.
(32) Lee, J.; Urban, A.; Li, X.; Su, D.; Hautier, G.; Ceder, G. *Science* **2014**, *343*, 519−522.
(33) Xu, Y.; Han, X.; Zheng, L.; Yan, W.; Xie, Y. *J. Mater. Chem.* **2011**, *21*, 14466−14472.

DOI: 10.1021/acs.nanolett.5b00284
Nano Lett. 2015, 15, 2180−2185